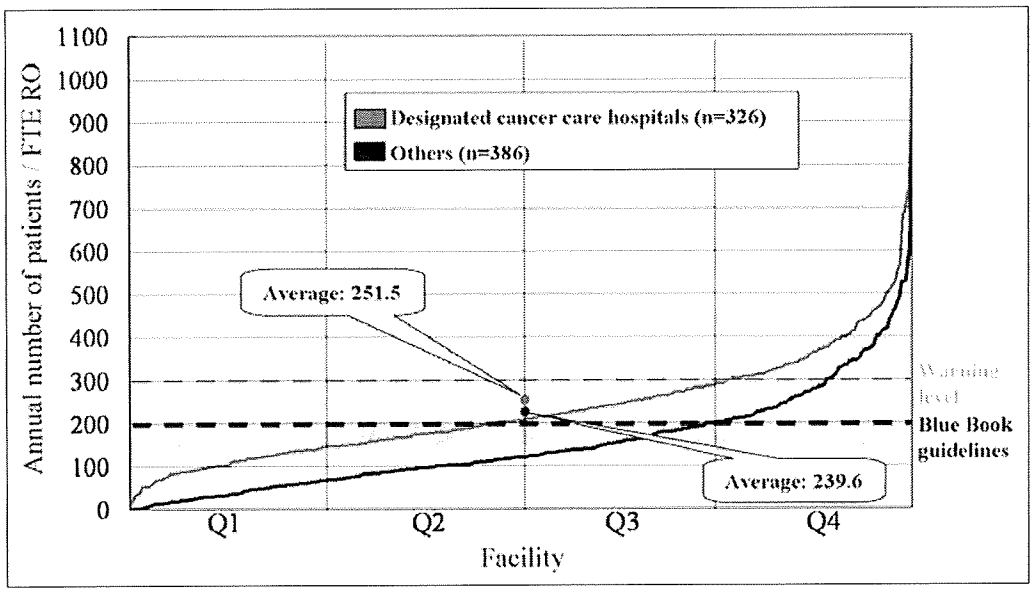

Fig. 1　Distribution of annual patient loads/FTE radiation oncologist in designated cancer care hospitals and other radiotherapy facilities. Horizontal axis represents facilities arranged in order of increasing value of the annual number of patients/FTE radiation oncologist within the facilities.

は，結局カルテを取り寄せたり，診療端末(HIS)上でデータを参照する必要があるのが現状である．これらは，さらにDBへの情報入力のモチベーションを下げる要因となっている．いくら優れたDBを構築しても，正確な情報が入力されなければ無意味である．

放射線治療の装備については整備改善が徐々に進んできているが，マンパワー不足はいまだにあまり改善されていない[4)-6)]．2005年の構造調査時点では，IMRTが可能なリニアックのうち，実際にIMRTが施行されていたのはわずか6%であり，マンパワー不足がその最大の要因であるものと思われた[7)]．

このマンパワー不足による放射線腫瘍医の加重な負担を解消するためには，放射線腫瘍医の増員が根本的な解決法として最も望まれるが，別のアプローチとして，JASTROデータベース委員会やIHE-J ROの活動などによって，放射線治療部門のワークフローの標準化が進めば，上記の各システム間のデータ連携などの問題が解消され，情報の共有化が可能となり，放射線腫瘍医の負担を軽減できるという方法も考えられる．その意味で今後もJASTROとしてIHE-J ROの活動を支援し，連携をとって活動を続けていくこととしている．

がん登録は，がんに関する情報を収集し，解析するためのシステムであるが，地域がん登録，院内がん登録，臓器別がん登録の3タイプに分けられる[10)]．これらは，それぞれ目的や役割が異なっている．日本においては，地域がん登録が1950年代から主に県単位で開始され，1992年に地域がん登録全国協議会が発足した[11)]．2007年現在，全国47のうちの35都道府県と1市において登録が行われている．法的な強制力はないこともあって，すべての地方自治体で施行されているわけではないが，がんの罹患率の推計や生存率の集計に役立てられている．院内がん登録は，現在は限られた病院でのみ行われているのが現状であるが，がん診療連携拠点病院においては，その登録が義務化されている．がん診療連携拠点病院が診療を行っているがん患者の割合は県によって異なると考えられ，70%程度を担当していると思われる県もあれば，25%程度にとどまっている地方自治体もあるとされている[10)]．臓器別がん登録は，特定の臓器がんにおいて，学会や研究グループレベルで登録が行われているものであり，他の2つと比較すると，より詳細なデータが集積されている[10)]．これらのがん登録間では，院内がん登録から地域がん登録へは情報の流れがあるが，臓器別がん登録とは情報の連携がなされていない．また，地域がん登録の中でも，登録内容の標準化が十分に進んでいないという問題も指摘されている．

米国では，National Cancer Database(NCDB)が1989年から開始され，現在では米国内の1,430以上の病院から新規がん患者の約70%(年約94万人)が登録されており，これまでに2,100万人分以上のデータが蓄積されている世界最大規模のがん登録データベースである[12)]．データは各施設の認定腫瘍登録士がまとめて提出し，QAチェックを受けている．このNCDBを用いた多数の研究論文が発表されており，がんの疫学から治療法の傾向，治療成績，癌治療の品質指標の確立など，幅広い分野にわたって役立てられており，がん治療の質の向上に貢献している．

日本の放射線治療の分野に関しては，前記のJASTROによる構造調査が行われており，また，診療内容や治療成績

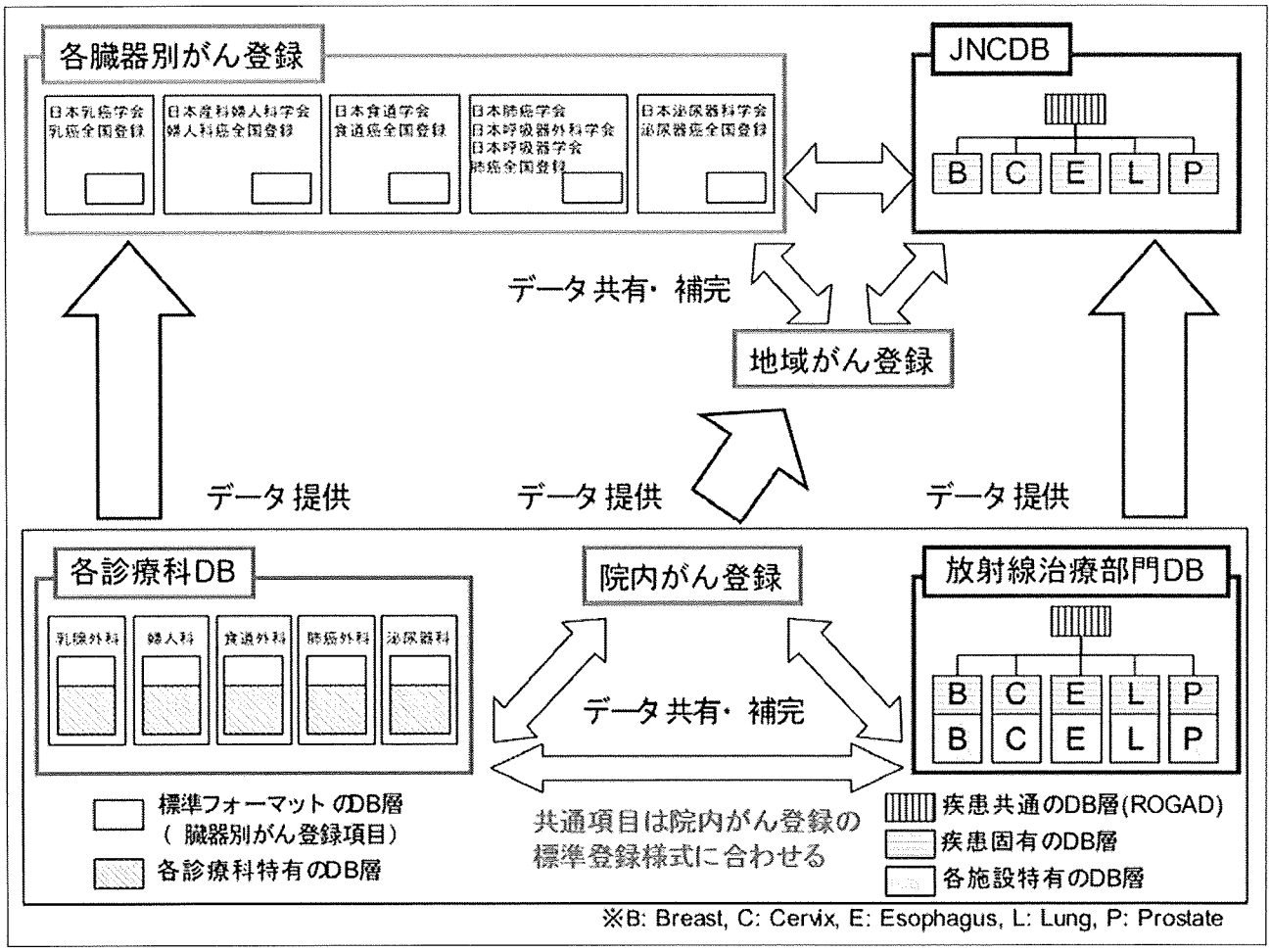

Fig. 2　Future direction of cancer registration system and cancer database system.

についてもPatterns of Care Study(PCS)である程度調査されているが[13]，十分な治療成績の情報を集積した調査としてのNCDBのようなものが，まだ整備されていない．NCDBは，がん治療のprocessとoutcomeの改善のためのquality indicatorとして使われている．現在，手島班においてJapanese National Cancer Database(JNCDB)を構築する準備が進められている[7]．Fig. 2にJNCDBを含めた各がん登録間の連携についての将来構想を示す．放射線治療部門は臓器横断的にデータを持っているため，他のがん登録や各施設の診療科DBと情報をうまく共有できれば，質の高いデータが各登録で補完できると考えられる．この中で，診療科DBや部門DBに関しては，IHE-J ROおよびJASTROデータベース委員会と連携して議論が行われており，より良いDBを提供できるように今後も改訂を継続していく予定となっている．

IHE-J ROの整備やJASTROデータベース委員会の活動等により，各システム間の連携，情報の共有がうまく行われるようになり，さらには，その情報が臓器別がん登録やJNCDBといった形で，全国的に集計，解析され，単なる疫学調査にとどまらず，治療成績の評価にもつながるようなシステムが構築されれば，DB入力の意義を実感できるようになるであろう．臨床家のために役立つ全国的がん診療評価システムの構築実現が望まれる．

文　献

1) 豊田達也，青木幸昌，小塚拓洋，他：電子カルテシステムの読む立場からの有用性の検討．日放腫会誌 **12**：293-305，2000.
2) 稲邑清也，原内　一，日本放射腺腫瘍学会データベース委員会委員：放射腺腫瘍学広域データベースROGAD(Radiation Oncology Greater Area Database)の報告―その活動の終結にあたって―．日放腫会誌 **19**：171-179，2007.
3) http://www.jastro.jp/report/topic/070419.html
4) Teshima T, Numasaki H, Shibuya H, et al.: Japanese structure survey of radiation oncology in 2005 based on institutional stratification of patterns of care study. *Int J Radiat Oncol Biol Phys* **72**: 144-152, 2008.
5) 手島昭樹，沼崎穂高，渋谷　均，他：全国放射線治療施設の2005年定期構造調査報告(第2報)．日放腫会誌 **19**：193-205，2007.

6) 手島昭樹，沼崎穂高，渋谷　均，他：全国放射線治療施設の2005年定期構造調査報告(第1報)．日放腫会誌 **19**：181-192，2007.
7) Numasaki H, Teshima T, Shibuya H, et al.: National Structure of Radiation Oncology in Japan with Special Reference to Designated Cancer Care Hospital. *Int J Clin Oncol, in press*, 2008.
8) Inter-Society Council for Radiation Oncology: Radiation oncology in integrated cancer management 1991(日本語訳：廣川　裕，井上俊彦，池田　恢(訳)「統合的癌治療における放射線腫瘍学」，(略称)「ブルーブック」)．放射線科専門医会，1993.
9) 日本PCS作業部会(厚生労働省がん研究助成金計画研究班14-6)：がんの集学治療における放射線腫瘍学―医療実態調査研究に基づく放射線治療の品質確保に必要とされる基準構造―．2005.
10) Sobue T: Current activities and future directions of the cancer registration system in Japan. *Int J Clin Oncol* **13**: 97-101, 2008.
11) Okamoto N: A history of the cancer registration system in Japan. *Int J Clin Oncol* **13**: 90-96, 2008.
12) Bilimoria KY, Stewart AK, Winchester DP, et al.: The National Cancer Data Base: a powerful initiative to improve cancer care in the United States. *Ann Surg Oncol* **15**: 683-690, 2008.
13) Teshima T: Patterns of care study in Japan. *Jpn J Clin Oncol* **35**: 497-506, 2005.

要旨：放射線治療に関する情報をどのように入力，管理，運用し，さらに有効活用していくかについては，まだまだ問題が多い．当院では，以前から放射線治療部門データベース(部門DB)が構築運用されていたが，実質上管理が困難な状態となり，Filemakerベースの DBに再構築した．現状に合わなくなったテーブルや項目を割愛したり，放射線治療広域データベースROGADに含まれる項目を加えたりすることにより，JASTROの構造調査への対応や，将来の全国規模のデータ収集への対応も可能となることを目指した．しかし，実際にはデータの入力もれや，入力方法の誤りなどのために，今回のJASTRO構造調査に対応した正確なデータを抽出することはできなかった．また，当院では，放射線治療に関するRISが更新され，その入力が必須となったが，部門DBとの連携がなく，情報入力の負担が増えている．がん診療連携拠点病院に指定され，院内がん登録も本格的に開始されたが，やはり部門DBとの連携がない状況である．このように当院内だけにおいても，情報の共有が行われておらず，現場の負担は増え続けている．この状況で情報入力が義務化されても，その意義を感じられなければ，実際の情報入力者である担当医のモチベーションは下がり，情報の正確性が低下してしまうという悪循環に陥りかねない．IHE-J ROの整備やJASTROデータベース委員会の活動等により，各システム間の連携，情報の共有がうまく行われるようになり，さらには，その情報が臓器別がん登録やJNCDB(Japanese National Cancer Database)といった形で，全国的に集計，解析され，単なる疫学調査にとどまらず，治療成績の評価にもつながるようなシステムが構築されれば，DB入力の意義を実感できるようになるであろう．臨床家のために役立つ全国的がん診療評価システムの構築実現が望まれる．

Application of laser-accelerated protons to the demonstration of DNA double-strand breaks in human cancer cells

A. Yogo,[1,a)] K. Sato,[2] M. Nishikino,[1] M. Mori,[1] T. Teshima,[2] H. Numasaki,[2] M. Murakami,[3] Y. Demizu,[3] S. Akagi,[3] S. Nagayama,[3,4] K. Ogura,[1] A. Sagisaka,[1] S. Orimo,[1] M. Nishiuchi,[1] A. S. Pirozhkov,[1] M. Ikegami,[1] M. Tampo,[1] H. Sakaki,[1] M. Suzuki,[1] I. Daito,[1] Y. Oishi,[5] H. Sugiyama,[1,6] H. Kiriyama,[1] H. Okada,[1] S. Kanazawa,[1] S. Kondo,[1] T. Shimomura,[1] Y. Nakai,[1] M. Tanoue,[1,6] H. Sasao,[1,6] D. Wakai,[1,6] P. R. Bolton,[1] and H. Daido[1]

[1]*Photo-Medical Research Center, JAEA, Kyoto 619-0215, Japan and Advanced Photon Research Center, JAEA, Kyoto 619-0215, Japan*

[2]*Department of Medical Physics and Engineering, Graduate School of Medicine, Osaka University, Osaka 565-0871, Japan*

[3]*Hyogo Ion Beam Medical Center, Hyogo 679-5165, Japan*

[4]*Shin Nippon Biomedical Laboratories Ltd., Kagoshima 891-1394, Japan*

[5]*Central Research Institute of Electric Power Industry, Kanagawa 240-0196, Japan*

[6]*Nippon Advanced Technology Co., Ltd., Ibaraki 319-1112, Japan*

(Received 13 February 2009; accepted 16 March 2009; published online 7 May 2009)

We report the demonstrated irradiation effect of laser-accelerated protons on human cancer cells. *In vitro* (living) A549 cells are irradiated with quasimonoenergetic proton bunches of 0.8–2.4 MeV with a single bunch duration of 15 ns. Irradiation with the proton dose of 20 Gy results in a distinct formation of γ-H2AX foci as an indicator of DNA double-strand breaks generated in the cancer cells. This is a pioneering result that points to future investigations of the radiobiological effects of laser-driven ion beams. Unique high-current and short-bunch features make laser-driven proton bunches an excitation source for time-resolved determination of radical yields. © *2009 American Institute of Physics*. [DOI: 10.1063/1.3126452]

After the initial proposal by Wilson,[1] it has been widely recognized that the use of particle ion beams in cancer radiotherapy has the physical advantage of delivering highly local dose distributions due to the well-known inherent Bragg peak phenomenon of energy deposition. Further benefit of the ion beam therapy (IBT) was found with increased relative biological effectiveness (RBE) within the Bragg peak region.[2]

Recently, high-intensity lasers have been suggested as a potential cost-saving alternative[3] to conventional ion accelerators for the radiotherapy. When a laser pulse with intensity well exceeding 10^{18} W/cm^2 interacts with a foil target, the laser field accelerates a significant number of electrons to relativistic velocities. Some of these "hot" electrons pass through the foil generating a strong electrostatic field exceeding 1 TV/m,[4–6] at the rear (downstream) surface, which can surpass the ion-acceleration field typical of conventional accelerators by six orders of magnitude. A unique feature of laser acceleration is the extremely high peak current attributed mostly to the short duration of a single proton bunch. In recent works,[7,8] single high-intensity laser pulses have produced proton bunches of charge level at 10^{11}, corresponding to ~1 kA peak ion currents 1 mm from the target. However, there has been no experimental work investigating biological effects of such high-current, short-bunch laser-driven ion beams.

In this letter, we describe a laser-driven ion irradiation apparatus for biological studies. We demonstrate DNA double-strand breaks (DSB) of *in vitro* human cancer cells and discuss the potential of the laser-driven ion beam as a short-pulse excitation source for biochemical reactions.

The experiment was performed using the J-KAREN (Ref. 9) Ti:sapphire laser system at JAEA. The laser pulses of 0.6 J energy and 35 fs duration are focused to a peak intensity of 5×10^{19} W/cm^2 onto a thin foil target, which is continuously fed by a servomotor, providing a "fresh" target surface for each laser shot. The laser pulses are delivered at a repetition rate of 1 Hz. As illustrated in Fig. 1(a), such intense laser irradiation generates energetic protons that diverge from the rear side of the target with a half-cone angle of ~10° with respect to the normal of the foil rear surface. The proton beam has a continuous distribution of the energy up to 2.5 MeV, as illustrated in Fig. 2(a) with a gray line.

Accompanying proton emission, are electrons and x rays that are generated simultaneously from the laser-induced plasma. In order to remove them, we used a pair of dipole magnets with magnetic fields of 0.04 T oriented antiparallel

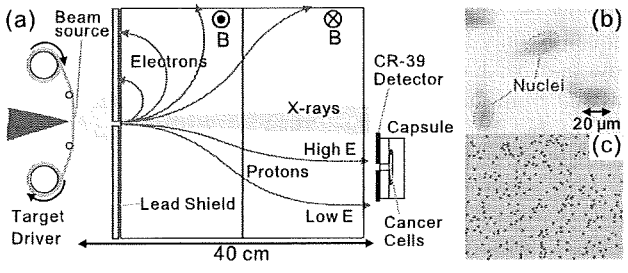

FIG. 1. (Color) (a) A schematic drawing of experimental setup. (b) An image of cancer cells taken by a microscope. (c) A spatial distribution of protons detected by CR-39 in a single laser shot. Each red point represents a single proton bombardment. The screen size is set to be same as that in the frame (b).

[a)]Electronic mail: yogo.akifumi@jaea.go.jp.

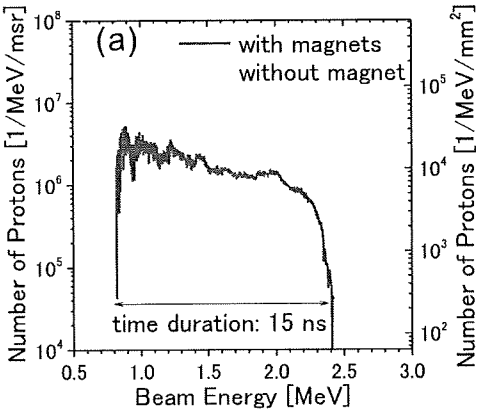

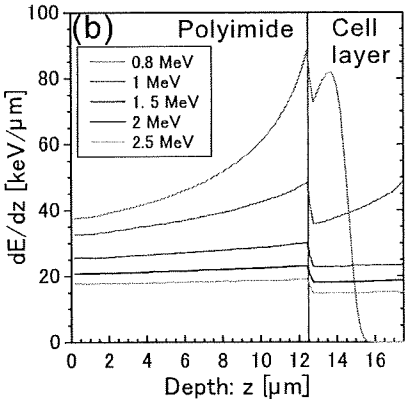

FIG. 2. (Color) (a) Typical energy spectra of proton beams obtained with the magnetic fields (blue line) and without the magnetic fields (gray line). Each spectrum shows the number of protons obtained in a single laser shot. (b) The results of 3D Monte Carlo simulations: distributions of electronic energy loss $d\mathcal{E}/dz$ as a function of the depth z.

to each other, as shown in Fig. 1(a). Protons, electrons and x rays enter the first magnetic field through a 1-mm-wide one-dimensional aperture made on a lead shield. Protons are steered in the opposite direction to that of the electrons, while x rays propagate straight through along the target normal axis. In the present experiment, electron energies are observed to be lower than 2 MeV, corresponding to a Larmor radius of about 20 cm; meaning that they are completely swept away from the normal axis and the protons. On the other hand, the proton trajectory is steered slightly by the first magnetic field, and again by the second one, such that transmitted proton trajectories are laterally displaced from the target normal axis by an energy-dependent distance.

The experimental setup as shown in Fig. 1 is placed in a vacuum chamber and the irradiated cancer cell culture is enclosed in a specially designed capsule. As shown in Fig. 1(a), the capsule consists of a vessel for culture solution and a 12.5-μm-thick polyimide foil window for protons. The foil window and the vessel are sealed by a silicon rubber o-ring that is fixed by screws with a lid having a pinhole of 2 mm in diameter on its center. We use human lung cancer cells: A549 pulmonary adenocarcinoma, the microscopic image of which is shown in Fig. 1(b). The average cell nucleus is of width $\sim$20 μm and thickness of $\sim$5 μm, as determined by a laser-probe microscope (Keyence VK-9700 Generation II). The *in vitro* A549 cells are cultured directly on the surface of the polyimide foil. Protons irradiate the cells after penetrating the polyimide film. The polyimide foil is strong enough to sustain a 1 atm pressure difference across it (the culture solution is at 1 atm). During the proton irradiation, we placed the capsule at the exit of the magnet pair, shifting the capsule window by 5 mm from the center axis of the magnets. Consequently only higher-energy protons enter the capsule window and irradiate the cells, as shown in Fig. 1(a). X rays emitted from the target emerging around the center axis are cut off by the lead shields. They do not radiate the cell samples.

The energy and number of protons are determined by a time-of-flight spectrometer[10] located downstream of the magnets, with the capsule temporarily removed and a different 2-mm-wide aperture placed at the same position as the capsule window. A typical incident energy spectrum obtained at this location is shown as a blue line in Fig. 2(a). The figure clearly shows that the energy spectrum looses its lowest-energy components (<0.8 MeV, as seen in the gray line) when the magnets are used. The proton bunch duration at the capsule position is about 15 ns. Protons with the energies above 0.8 MeV can penetrate the polyimide window to irradiate cancer cells. The measured number of protons per bunch varies by less than 20% (bunch-to-bunch) at the 1 Hz repetitive rate.

The number of protons corroborated during cell irradiation by an ion-track detector (CR-39), which is covered with another 12.5-μm-thick polyimide foil and placed beside the capsule window. Protons penetrating the foil window impinge on the CR-39, as shown in Fig. 1(c). Each red point in the image represents the bombardment of one proton, which is visualized with software postprocessing. The screen size (80×110 μm^2) is set to be same as that in Fig. 1(b). The average number of protons per bunch irradiating the cells is measured to be $2.5\pm0.5\times10^4$ with the energy spread from 0.8 to 2.4 MeV.

The proton dose is estimated from the measured proton number and energy spectrum per bunch using a Monte Carlo simulation in the TRIM code.[11] We calculate the energy loss of the protons in a three-dimensional (3D) target consisting of the layers of 12.5-μm-thick polyimide and 5-μm-thick liquid water, which is assumed to be equivalent to the layer of the cancer cells planted on the polyimide-foil window.

Figure 2(b) shows the calculated z dependent proton energy loss distribution $d\mathcal{E}/dz$ (to the target electrons) for several beam energies in the range of $\mathcal{E}$=0.8–2.5 MeV. Here, the depth of z=0 μm represents the entrance (upstream) surface of the polyimide window. We note that protons with energies of $\mathcal{E}$=0.8 and 2.5 MeV leave the bottom of the polyimide window with energies of 0.16 and 2.17 MeV, respectively, and encounter the cancer cells. For $\mathcal{E}\geq1.5$ MeV, the electronic energy loss $d\mathcal{E}/dz$ is about 20 keV/μm in the cell layer ($12.5\leq z\leq17.5$ μm). At lower incident energy ($\mathcal{E}$=0.8 MeV), protons have the highest $d\mathcal{E}/dz$ value and are stopped in the cell layer. The $d\mathcal{E}/dz$ used in this work is equivalent to the linear energy transfer (LET). As illustrated in Fig. 2(a), more than 85% of the protons have energy above the 1 MeV level. Belli *et al.*[12] has reported that RBE exhibits a strong dependency on the LET of the primary ions: for protons, the RBE takes a maximum with the LET range of 20–30 keV/μm. Hence, in the present experiment, the cancer cells are irradiated predominantly with protons of energy near the RBE maximum.

The energy E_d deposited on the cell layer is determined by integrating the stopping power according to: $E_d(\mathcal{E})=\int_{z_1}^{z_2}(d\mathcal{E}/dz)dz$. Here, $d\mathcal{E}/dz$ is in units of keV/μm for each incident beam energy ε and integrated over the cell layer

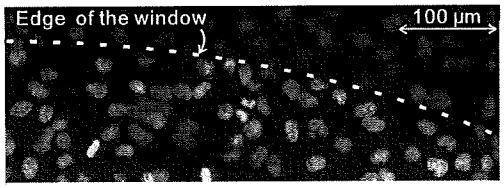

FIG. 3. (Color) γ-H2AX focus formation induced by irradiation of laser-accelerated protons with 20 Gy. γ-H2AX and nucleus are stained with anti-γ-H2AX antibody (green) and DAPI (blue).

from $z_1=12.5$ μm to $z_2=17.5$ μm. Therefore absorbed dose D of a single proton bunch is estimated (in Gy units) by the following relation: $D=\int d\mathcal{E}[E_d(\mathcal{E})\cdot N(\mathcal{E})]/[(z_2-z_1)\cdot Q]\cdot 1.602\times 10^{-7}$, where $N(\mathcal{E})$ is the proton fluence distribution at the capsule entrance {in units of $\mathrm{mm}^{-2}\,\mathrm{MeV}^{-1}$ [see the right vertical axis of Fig. 2(a)]} and Q is the mass density of liquid water in $\mathrm{g/cm}^3$. We determine the absorbed dose of protons to be $D\simeq 0.1\pm 0.02$ in a single laser shot.

DNA DSB induced on A549 are investigated by using phosphorylated histone H2AX immunostaining method. It has been recognized[13] that the H2AX phosphorylation along the DNA strand corresponds only with the site of DSB. Therefore, the remark of phosphorylated H2AX in the nuclei (termed as γ-H2AX focus formation) can be used as a criterion for DNA DSB. Figure 3 illustrates the results of γ-H2AX immunofluorescence staining obtained for the proton irradiation with 20 Gy. The proton dose was accumulated with 200 laser shots at a repetition rate of 1 Hz. Here, nuclei and γ-H2AX foci are stained with blue and green, respectively. One can easily find that γ-H2AX focus formation is detected in the nuclei. Moreover, the region of γ-H2AX positive exhibits a clear boundary along the edge of the capsule window; indicating that γ-H2AX foci are generated only in the nuclei that were irradiated with the protons. We note that we have confirmed that γ-H2AX foci are generated independently of the culture condition (see supplemental materials).[14] Therefore, we conclude that DNA DSB were induced by the irradiation of the laser-accelerated protons.

In what follows we discuss the inherent potential of laser-accelerated protons. In this study $\sim 2.5\times 10^4$ laser-driven protons irradiate a 1 mm^2 cell layer within a time interval of only 15 ns. We then estimate the proton flux to be $\sim 10^3$ $\mathrm{mm}^{-2}\,\mathrm{ns}^{-1}$. On the other hand, in a typical operation of IBT,[14] tumors are irradiated with the beam with flux of $\sim 10^{-4}$ $\mathrm{mm}^{-2}\,\mathrm{ns}^{-1}$ and a proton bunch duration of 0.4 s. Within 15 ns the present laser-driven source delivers protons with a proton number comparable to that delivered with 0.4 s duration pulse in the IBT operation. The dynamics differ by seven orders of magnitude for these cases. In radiation chemistry, it is recognized[15] that the chemical transformation induced by the energetic ions continues over the time scale of 10^{-10} to 10^{-6} s, which spans the duration of our laser-driven source of 10^{-8} s. Therefore, the laser-driven proton bunches can be a potential excitation source for the time-resolved measurements of chemical reactions including the formation and dissipation processes of hydroxyl (OH) radicals[16] induced by the ion irradiation. A study such as ion-pulse radiolysis enabled by such short irradiation durations can explore the relationship between the fundamental chemical reactions of radiation effects and the ensuing biological processes.

In conclusion, we have shown that DNA DSB are generated in human cancer cells irradiated with the high-current and short-bunch ion beams driven by a laser system. It is interesting to note that about 8 proton particles, in average, were delivered to the single cancer cell nucleus in duration of the single beam bunch of 15 ns. The laser-driven *table-top* ion-irradiation apparatus will open a new field of radiobiological science and applications.

This work is supported by Special Coordination Funds for Promoting Science (SCF) and "Mono-energetic quantum beam science with PW lasers" project commissioned by the Ministry of Education, Culture, Sports, Science and Technology (MEXT) of Japan.

[1]R. R. Wilson, Radiology **47**, 487 (1946).
[2]G. Kraft, M. Scholz, and U. Bechthold, Radiat. Environ. Biophys. **38**, 229 (1999).
[3]S. V. Bulanov, T. Zh. Esirkepov, V. S. Khoroshkov, A. V. Kuznetsov, and F. Pegoraro, Phys. Lett. A **299**, 240 (2002).
[4]M. Borghesi, J. Fuchs, S. V. Bulanov, A. J. Mackinnon, P. K. Patel, and M. Roth, Fusion Sci. Technol. **49**, 412 (2006).
[5]B. M. Hegelich, B. J. Albright, J. Cobble, K. Flippo, S. Letzring, M. Paffett, H. Ruhl, J. Schreiber, R. K. Schulze, and J. C. Fernández, Nature (London) **439**, 441 (2006).
[6]J. Fuchs, P. Antici, E. d'Humieres, E. Lefebvre, M. Borghesi, E. Brambrink, C. A. Cecchetti, M. Kaluza, V. Malka, M. Manclossi, S. Meyroneinc, P. Mora, J. Schreiber, T. Toncian, H. Pepin, and P. Audebert, Nat. Phys. **2**, 48 (2006).
[7]M. Nishiuchi, H. Daido, A. Yogo, S. Orimo, K. Ogura, J. Ma, A. Sagisaka, M. Mori, A. S. Pirozhkov, H. Kiriyama, S. V. Bulanov, T. Zh. Esirkepov, I. W. Choi, C. M. Kim, T. M. Jeong, T. J. Yu, J. H. Sung, S. K. Lee, N. Hafz, K. H. Pae, Y.-C. Noh, D.-K. Ko, J. Lee, Y. Oishi, K. Nemoto, H. Nagatomo, K. Nagai, and H. Azuma, Phys. Plasmas **15**, 053104 (2008).
[8]T. E. Cowan, J. Fuchs, H. Ruhl, A. Kemp, P. Audebert, M. Roth, R. Stephens, I. Barton, A. Blazevic, E. Brambrink, J. Cobble, J. Fernandez, J.-C. Gauthier, M. Geissel, M. Hegelich, J. Kaae, S. Karsch, G. P. Le Sage, S. Letzring, M. Manclossi, S. Meyroneinc, A. Newkirk, H. Pepin, and N. Renard-LeGalloudec, Phys. Rev. Lett. **92**, 204801 (2004).
[9]H. Kiriyama, M. Mori, Y. Nakai, T. Shimomura, M. Tanoue, A. Akutsu, H. Okada, T. Motomura, S. Kondo, S. Kanazawa, A. Sagisaka, J.-L. Ma, I. Daito, H. Kotaki, H. Daido, S. V. Bulanov, T. Kimura, and T. Tajima, Opt. Commun. **282**, 625 (2009).
[10]A. Yogo, H. Daido, S. V. Bulanov, K. Nemoto, Y. Oishi, T. Nayuki, T. Fujii, K. Ogura, S. Orimo, A. Sagisaka, J.-L. Ma, T. Zh. Esirkepov, M. Mori, M. Nishiuchi, A. S. Pirozhkov, S. Nakamura, A. Noda, H. Nagatomo, T. Kimura, and T. Tajima, Phys. Rev. E **77**, 016401 (2008).
[11]J. F. Ziegler, J. P. Biersack, and M. D. Ziegler, *SRIM - The Stopping and Range of Ions in Matter* (SRIM, Maryland, 2008).
[12]M. Belli, R. Cherubini, S. Finotto, G. Moschini, O. Sapora, G. Simone, and M. A. Tabocchini, Int. J. Radiat. Biol. **55**, 93 (1989).
[13]A. J. Downs, C. M. Nussenzweig, and A. Nussenzweig, Nature (London) **447**, 951 (2007).
[14]See EPAPS Document No. E-APPLAB-94-001918 for supplemental materials. For more information on EPAPS, see http://www.aip.org/pubservs/epaps.html.
[15]A. Mozumder, in *Charged Particle Tracks and Their Structure. Advances in Radiation Chemistry 1, 1*, edited by M. Burton and J. L. Magee (Wiley, New York, 1969).
[16]M. Taguchi, A. Kimura, R. Watanabe, and K. Hirota, Radiat. Res. **171**, 254 (2009).

Int. J. Radiation Oncology Biol. Phys., Vol. 75, No. 2, pp. 571–579, 2009

0360-3016/09/$–see front matter

ELSEVIER

doi:10.1016/j.ijrobp.2009.02.088

5TH JUCTS AND THE 5TH S. TAKAHASHI MEMORIAL INTERNATIONAL JOINT SYMPOSIUM

A PRELIMINARY STUDY OF IN-HOUSE MONTE CARLO SIMULATIONS: AN INTEGRATED MONTE CARLO VERIFICATION SYSTEM

NOBUTAKA MUKUMOTO, M.S.,* KATSUTOMO TSUJII, M.S.,* SUSUMU SAITO, M.S.,* MASAYOSHI YASUNAGA, M.S.,* HIDEKI TAKEGAWA, M.S.,† TOKIHIRO YAMAMOTO, PH.D.,* HODAKA NUMASAKI, PH.D.,* AND TERUKI TESHIMA, M.D., PH.D.*

*Department of Medical Physics and Engineering, Osaka University Graduate School of Medicine, Suita, Osaka, Japan; and †Department of Radiation Oncology, Osaka Medical Center for Cancer and Cardiovascular Diseases, Higashinari-ku, Osaka, Japan

Purpose: To develop an infrastructure for the integrated Monte Carlo verification system (MCVS) to verify the accuracy of conventional dose calculations, which often fail to accurately predict dose distributions, mainly due to inhomogeneities in the patient's anatomy, for example, in lung and bone.

Methods and Materials: The MCVS consists of the graphical user interface (GUI) based on a computational environment for radiotherapy research (CERR) with MATLAB language. The MCVS GUI acts as an interface between the MCVS and a commercial treatment planning system to import the treatment plan, create MC input files, and analyze MC output dose files. The MCVS consists of the EGSnrc MC codes, which include EGSnrc/BEAMnrc to simulate the treatment head and EGSnrc/DOSXYZnrc to calculate the dose distributions in the patient/phantom. In order to improve computation time without approximations, an in-house cluster system was constructed.

Results: The phase-space data of a 6-MV photon beam from a Varian Clinac unit was developed and used to establish several benchmarks under homogeneous conditions. The MC results agreed with the ionization chamber measurements to within 1%. The MCVS GUI could import and display the radiotherapy treatment plan created by the MC method and various treatment planning systems, such as RTOG and DICOM-RT formats. Dose distributions could be analyzed by using dose profiles and dose volume histograms and compared on the same platform. With the cluster system, calculation time was improved in line with the increase in the number of central processing units (CPUs) at a computation efficiency of more than 98%.

Conclusions: Development of the MCVS was successful for performing MC simulations and analyzing dose distributions. © **2009 Elsevier Inc.**

Monte Carlo simulations, Verification, Photon beam, High precision radiotherapy.

INTRODUCTION

Improvements in dose delivery techniques have rendered it possible to point the dose exactly to the tumor volume and spare the surrounding normal tissues. However, beam delivery in radiotherapy has become increasingly complex since the advent of three-dimensional conformal radiotherapy (3DCRT), intensity-modulated radiotherapy (IMRT), and stereotactic body radiotherapy (SBRT). Especially with these high-precision radiation therapies, accurate dose calculations are essential for radiotherapy planning. To meet this need, comparatively accurate dose calculation algorithms, such as the convolution/superposition method, have come into use for commercial treatment planning systems (1-3). However, these algorithms often fail to predict accurate dose distributions, mainly due to inhomogeneities in the patient's anatomy, for example, in lung and bone, and to several multileaf collimator (MLC)-specific effects, which include leakage of radiation, the tongue-and-groove effect, and beam hardening (4-10). For example, some conventional algorithms in widespread use for commercial treatment planning systems cause systematic errors exceeding 10% in the thoracic area (11). Although the accuracy required for dose computation is generally between 1% and 2%, major errors in the doses calculated by conventional dose algorithms

Reprint requests to: Teruki Teshima, M.D., Ph.D., Department of Medical Physics and Engineering, Osaka University Graduate School of Medicine, 1-7 Yamadaoka, Suita, Osaka 565-0871, Japan. Tel.: (+81) 6-6879-2570; Fax: (+81) 6-6879-2570; E-mail: teshima@sahs.med.osaka-u.ac.jp

This study was supported by Grant-in-Aid for Scientific Research 16390320 from the Japan Society for the Promotion of Science and Grants-in-Aid for Cancer Research 14-6 and 18-4 from the Ministry of Health, Labor and Welfare, Japan.

This work was presented in part at the 5th Annual Japan-US Cancer Therapy Symposium, Sendai, Japan, September 7-9, 2007.

Conflict of interest: none.

Acknowledgment—We thank Mr. Katsutaro Kaneko of Varian Medical Systems for providing detailed information for the Clinac series linear accelerator.

Received Sept 3, 2008, and in revised form Feb 18, 2009. Accepted for publication Feb 27, 2009.

reportedly exceeded that criterion (5, 12-15). These uncertainties concerning dose distributions may cause unintended geographic misses of the target or an overdosage to normal tissues due to the incorrect prediction of isodose coverage and may thus negatively affect the clinical outcome (16).

Monte Carlo (MC) simulation is the most accurate dose calculation method currently available, since it can accurately calculate realistic radiation transport through the accelerator treatment head, the MLC, and the patient's internal anatomy. Moreover, the MC method uses the only algorithm that considers all aspects of photon and electron transport within a heterogeneous situation. The most widely used MC code is EGSnrc, which includes EGSnrc/BEAMnrc and EGSnrc/DOSXYZnrc (17, 18). BEAMnrc is an MC user code for modeling the linear accelerator, and DOSXYZnrc is its counterpart for 3D absorbed dose calculations.

The purpose of this study was to develop an integrated MC dose calculation system, which we called the MC verification system (MCVS). In this paper, we describe in detail the key features of the MCVS and the results of dose calculation accuracy benchmarks.

METHODS AND MATERIALS

Overview of the MCVS

Figure 1 shows a schematic diagram of the usual calculation flow for plan verification. The MCVS consists of two MC codes, that is, EGSnrc/BEAMnrc, which simulates radiation transport through the complex geometry of the linear accelerator treatment head, and EGSnrc/DOSXYZnrc, which calculates the patient's heterogeneous internal anatomy. The MCVS has an interface with a commercial treatment planning systems (Eclipse, Varian Medical Systems, Palo Alto, CA) and reads the information needed for the MC simulation transferred in the DICOM-RT format. With the graphical user interface (GUI), the MC input files are auto-created, and the output files are then processed for display and/or analysis.

Linear accelerator head simulation

For this study, a 6-MV photon beam from a Varian Clinac 23EX unit was simulated with the EGSnrc/BEAMnrc code. The following modeled linear accelerator head components were used: target/backing, primary collimator, vacuum window, flattening filter, mirror, and jaws on the X and Y coordinates. The monitor ion chamber could be omitted from modeling since it had only a minor attenuating effect on the photon beam (19). Figure 2 shows the schema of the simulated geometry. The phase-space data (PSD) file was scored at a plane immediately behind the lower jaws. The mean electron beam energy incident on the target and the full width half maximum (FWHM) of the radial intensity distribution were set to 5.95 MeV and 0.8 mm, respectively. The FWHM of energy distribution was consistently 3% of the mean energy. The distributions of the energy and intensity were assumed to be Gaussian in shape.

For MC simulation, 4.0×10^7 electron histories were simulated. The photon and electron cutoff energies, PCUT and ECUT, of 0.010 MeV and 0.700 MeV were used for all simulations. The variance reduction technique directional bremsstrahlung splitting was used during head simulation with a splitting number of 500 while the electron was also split. The PSD file contained approximately 8.5×10^6 to 3.4×10^7 photons which corresponded to the 270 MB to 1.0 GB file size for 10×10, 20×20, and 30×30 cm^2 open fields.

Dose calculations for a water phantom

The EGSnrc/DOSXYZnrc was used to calculate doses for a phantom. The $50 \times 50 \times 50$ cm^3 simulated water phantom was divided

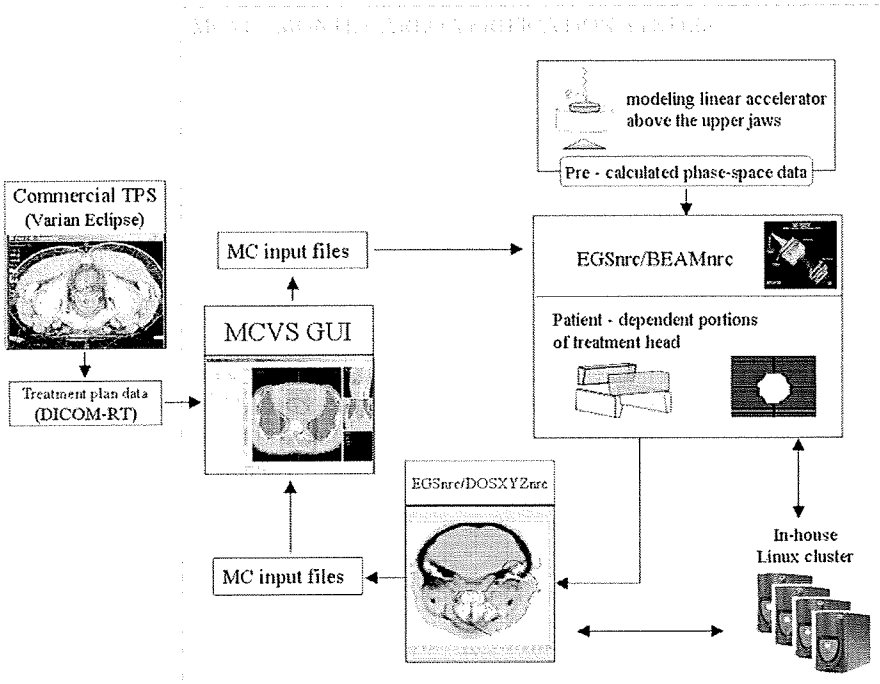

Fig. 1. Schematic diagram of the MCVS GUI showing the EGSnrc MC dose calculations in relation to an Eclipse treatment planning system. The MCVS GUI acts as an interface between EGSnrc and commercial treatment planning systems to read the radiotherapy planning data, create the patient phantom data, and analyze the output dose files calculated by EGSnrc.

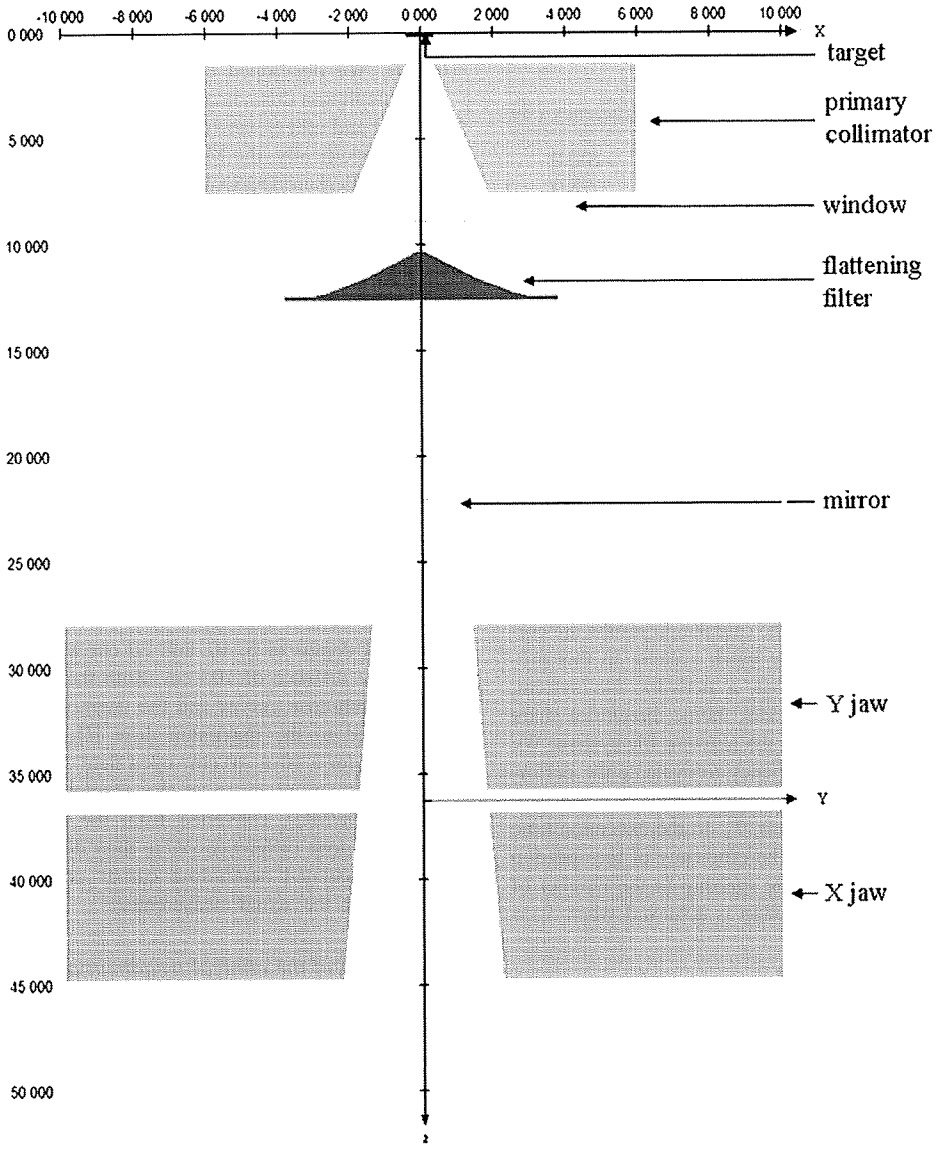

Fig. 2. Geometric schema illustrating the accelerator head components. *X* jaws are rotated 90° and are shown on the *y* coordinate.

into 1.0 cm, 2.0 cm, and 0.5 cm in the *x*, *y*, and *z* directions, respectively. The voxel deviation was small enough not to average the dose in a voxel. The jaws were set to produce 10 × 10, 20 × 20, and 30 × 30 cm^2 open fields at the surface of the phantom, and the source-to-surface distance was 100 cm. The stored PSDs were used as source inputs for the calculation of dose distributions in the phantom. A total of 2.5 × 10^9 histories were simulated in the DOSXYZnrc calculation, recycling the particles in the PSD file about 50 to 250 times to reduce statistical uncertainties. Depth–dose curves were calculated along the central axis, while *y* axis lateral dose profile curves were calculated at depths of 5, 10, and 20 cm in the phantom.

A history-by-history method was used to estimate uncertainties in BEAMnrc and DOSXYZnrc (20). This method involves grouping scored quantities (*e.g.*, doses, energy depositions) according to the primary history during a run and then determining the root mean square standard deviation for the mean of the groupings.

CT-based patient modeling

For in-patient MC dose calculation, treatment planning CT images were used to develop a voxel-based patient model. The process of converting CT data to an MC model (*i.e.*, materials and densities) was performed with a software program, as well as with CTCREATE software, distributed by the National Research Council. For the transformation of data from CT Hounsfield units into materials, four discrete intervals were defined corresponding to air, lung, soft tissue, and bone, which were obtained from the ICRU report (21). The mass densities were allocated at a range of 0 to 2.0 for discrete intervals.

Parallel calculation

The in-house-developed cluster consists of three calculation nodes which include two central processing units (CPUs)/node of an Intel Xeon processor with a speed of 3.4 GHz. The dual processors on each node are configured with 1.5 GB of random

Table 1. Speedup and efficiency of the in-house-developed cluster by total CPU time for the run*

No. of CPUs	Time (hr)	Speedup	Efficiency (%)
1	44.1	1.00	100.0
2	22.4	1.97	98.6
3	14.8	2.98	99.5
4	11.2	3.93	98.4
5	8.9	4.96	99.2
6	7.4	5.95	99.2

Abbreviations: Speedup = ratio of execution time on a single processor to the execution time using N processors. Efficiency = ratio of the speedup to the number of processors.

* The jobs were distributed to different processors.

access memory and therefore can operate as symmetrical multiprocessors on the node. The cluster uses the gigabyte-sized Ethernet network for the interconnection of nodes. In parallel processing, the EGSnrc/DOSXYZnrc code splits a job into smaller jobs which can be distributed to different processors, and all the split jobs use the original input file. The calculation results are collected and accumulated by a portable batch system. In this process, several files are transported via a network file system, which is a file sharing system. All nodes' home directories share the master node's home directory via the network file system. We used the indices of speedup and efficiency to evaluate the performance of the cluster. The speedup, S_N, can be defined as the ratio of execution time on a single processor, T_1, to the execution time using N processors, or $S_N = T_1/T_N$. The efficiency of the speedup can also be defined as the ratio of the speedup to the number of processors, or $E_N = S_N/N$. Ideal speedup is achieved when $S_N = N$ and $E_N = 100\%$.

GUI application

We developed an interface based on a computational environment for radiotherapy research(CERR) software version 3.0.2 using MATLAB software version 7.0.4 with an Image Processing Toolbox (The MathWorks, Natick, MA). CERR is a software platform developed at Washington University for the review and analysis of radiotherapy planning data (22, 23). Importing and displaying radiotherapy planning data from a wide variety of commercial or academic treatment planning systems, for example, RTOG and DICOM-RT formats, can be done with CERR. We developed certain features to analyze and display MC calculation dose data. Some of the programs were newly developed and others were developed by modifying the CERR program. Specifically, the MCVS GUI auto-creates patient phantom data for EGSnrc/DOSXYZnrc and the input files for EGSnrc/BEAMnrc and EGSnrc/DOSXYZnrc MC calculation parameters. These parameters were extracted from the plan data which contained the beam configuration (*i.e.*, the opening of jaws and the MLC, gantry angles, couch angles, and collimator angles). The GUI also imports the MC-calculated dose data to analyze these results in detail. These features were integrated into CERR.

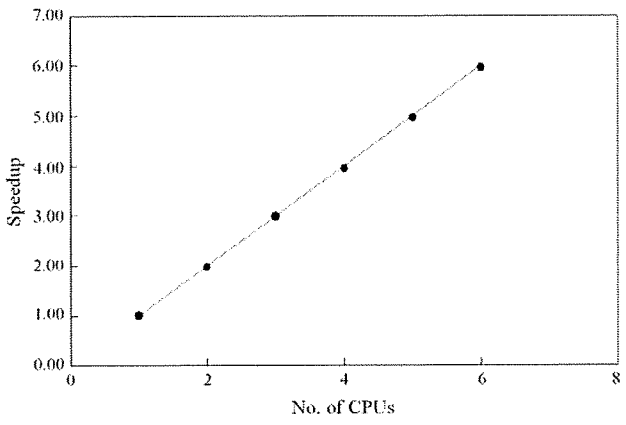

Fig. 3. Number of processors (CPUs) versus speedup (dots), using the cluster developed inhouse and theoretical figure (solid line).

Verification of the benchmarks under homogeneous conditions

The depth doses and lateral doses of the MCVS were benchmarked for comparison with the measurements and the calculated dose. The microionization chamber was used for measurements in the water phantom for a Varian Clinac 23EX linear accelerator installed at Osaka Medical Center for Cancer and Cardiovascular Diseases. Central axis depth–dose curves and lateral dose profile curves at depths of 5, 10, and 20 cm were obtained at a source-to-surface distance of 100 cm. Both the calculated and the measured depth-dose curves and the lateral dose profile curves were normalized to the maximum dose (D_{max}) value of the central axis dose for a 10 × 10 cm^2 open field. Therefore, the MC-calculated results were given in the absolute dose per monitor unit (MU) (cGy/MU), converted from the dose per source particle (24). The dose differences were then determined for comparison of the calculated depth-dose curves or the lateral dose profile curves with the actual measurements.

Validation of the clinical treatment plan

The MC dose calculation for a realistic clinical plan was performed, and the results were compared with those of Eclipse in order to verify the configuration of the beam and the patient/phantom in the MCVS. We also computed dose distributions with MC for a lung SBRT treatment plan. Four fractions of 12 Gy were prescribed to the isocenter by using an Eclipse/Helios system (Varian Medical Systems, Palo Alto, CA) for 6-MV photon beams with seven noncoplanar beams. The dose calculation algorithm employed in Eclipse was the pencil-beam convolution algorithm with modified Batho inhomogeneity corrections. Dose distributions were computed with the MCVS using treatment plan data transferred from Eclipse, and isodose curves and DVHs for the structures of interest were compared.

RESULTS

Parallel calculation

Table 1 shows the computation time, speedup, and efficiency values calculated for the cluster. The computation time decreased as the number of CPUs increased, while the speedup increased in proportion to the number of CPUs. The efficiency could be maintained at more than 98%. Figure 3 shows the relationship between the speedup and number of CPUs used in the simulation, indicating that the CPU time was shortest when six CPUs were used. The efficiency was 99.2%, so that these results were quite similar to those of the ideal situation.

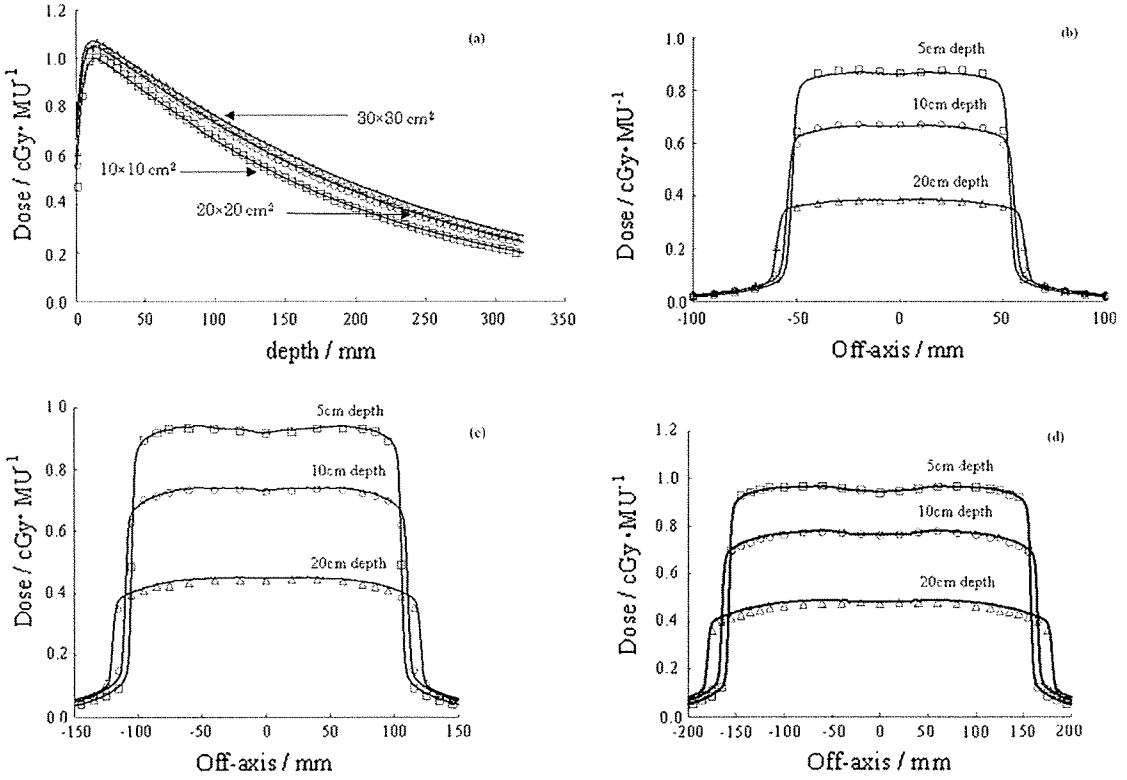

Fig. 4. Comparisons of measured (solid lines) and MC-calculated (symbols) 6-MV photon beam for 10 × 10, 20 × 20, and 30 × 30 cm^2 open fields. (a) Central axis depth–dose curves; (b) lateral dose profile curves for a 10 × 10 cm^2 open field; (c) lateral dose profile curves for a 20 × 20 cm^2 open field; (d) lateral dose profile curves for a 30 × 30 cm^2 open field.

Dose calculations under homogeneous conditions

Figure 4 a shows depth-dose curves at the central axis for 10 × 10, 20 × 20, and 30 × 30 cm^2 open fields. The calculated depth doses beyond the buildup region showed agreement of within 1% with the measurements for the depth-dose curves for all field sizes. Figure 4b to d shows lateral dose profile curves at 5-cm, 10-cm, and 20-cm depths for 10 × 10, 20 × 20, and 30 × 30 cm^2 open fields. The calculated lateral doses within the region of flatness agreed to within 1% with the measurements for lateral dose profile curves for all field sizes except the penumbra region. The MC-calculated dose profile curves for large fields yielded less steep dose gradients than measurements obtained at a greater depth. The statistical uncertainties for the simulated dose values at the edge of the lateral dose profile curves were 2.5%, and, except for the edge, the uncertainties including those for the depth-dose curves were within 1%.

Validation of the clinical treatment plan calculation

Figure 5 shows a comparison of the 6-MV photon beam dose distributions for a lung SBRT treatment plan calculated by MC and by Eclipse. For both calculations, the isodose lines show the absolute dose. The seven beams calculated by the MC method generated a dose distribution similar to that of Eclipse, which indicates that the configuration of the beams and the patient/phantom were satisfactorily implemented in the MCVS. There were some dose differences of about 5% between the MC and the Eclipse calculations within or near the lung anatomy. The 1σ statistical uncertainty for the MC results was generally 2%.

Figure 6 shows dose volume histograms (DVHs) for MC and Eclipse calculations on the MCVS GUI. In this figure, the DVHs for internal target volume and lung are shown, and the same data as that of the radiotherapy planning were used for these structure data. The dose index could be shown as the output next to DVHs, such as D_{mean}, D_{max}, and D_{min}, and furthermore, the dose which was irradiated at a certain percent volume, such as D95, and the percent volume at which the dose exceeding a certain dose was irradiated for a certain structure, such as V20, could also be shown as output with the MCVS GUI.

DISCUSSION

Several academic and commercial MC dose calculation systems have been developed (4, 25-39). These systems are summarized in Table 2 for comparison. The PEREGRINE system has been used with multiple processors and several variance reduction techniques to reduce the CPU time of the simulations (26). Several fast MC codes, such as VMC/xVMC, VMC++, DPM, MCV, and MCDOSE, have been developed (27-35). These codes employ a variety of variance reduction techniques and achieve reduction of CPU time by factors ranging from 2 to 48 compared with EGS4/PRESTA/DOSXYZ calculations,

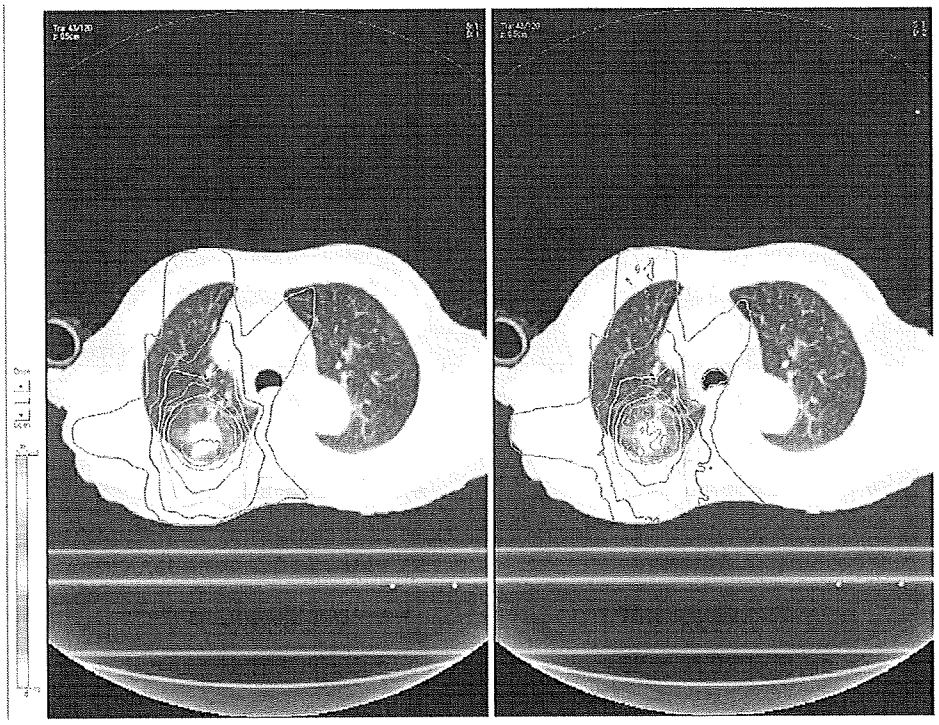

Fig. 5. Comparison of the 6-MV photon beam dose distributions for a lung SBRT treatment plan calculated by Eclipse (left panel) and MC (right panel) on the MCVS GUI. Four fractions of 12 Gy were prescribed to the isocenter. Isodose lines from 8 Gy to 48 Gy at intervals of 8 Gy are shown.

which corresponds approximately to EGSnrc (40). The MC method with its accurate dose computations is now becoming fast enough to be used in clinical settings. While the fast MC codes use various variance reduction technique s to reduce computation time, the results are only approximate, but with the cluster system, the MCVS could reduce computation time without such approximations. Parallel computation with the in-house-developed cluster achieved good performance at a computation efficiency of more than 98%. In Japan, the MCVS of Osaka University and the MCRTV of Kyoto University are the only two systems in existence, while several MC research groups in other

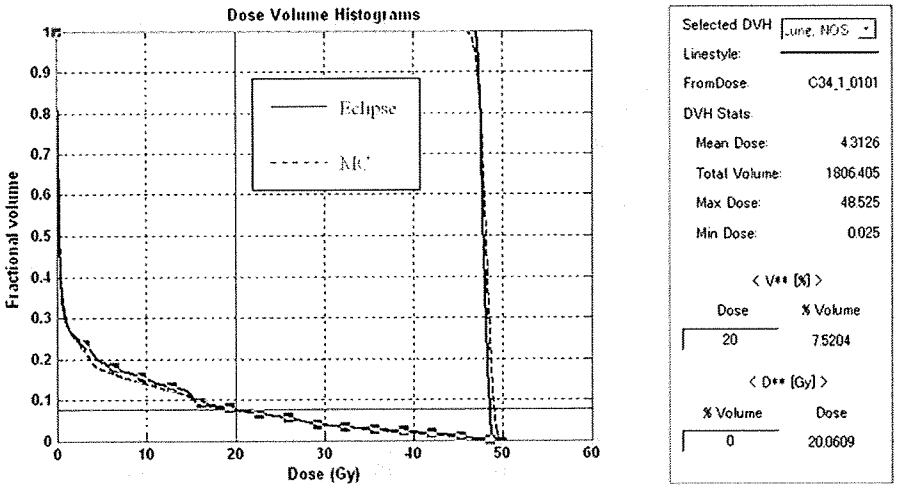

Fig. 6. The DVHs of internal target volume and lung calculated by DOSXYZnrc (dashed line) and by Eclipse (solid line) are shown. On the MCVS GUI, these structure data are identical to those of radiotherapy planning. The dose index can be displayed next to DVHs, such as D_{mean}, D_{max}, and D_{min}. Furthermore, the dose which was irradiated at a certain percent volume, such as D95, and the percent volume at which the dose exceeding a certain level was irradiated to a structure volume such as V20 can also be calculated on the MCVS GUI.

Table 2. Survey of academic and commercial MC dose calculation systems

Location or company (MC system)	MC code	Type of MC code	Calculation time (min)	Reference
Academic				
Osaka U (MCVS)	EGSnrc	Full	42.9 (7.2*)	
Kyoto U (MCRTV)	EGS4	Full	42.9	38
MSKCC	EGS4	Full		39
UCLA (RTMCNP)	MCNP	Full	60	4
McGill U (MMCTP)	EGSnrc + XVMC	Full + fast		37
Stanford U/FCCC (MCDOSE, MCSIM)	modified EGS4	Fast	1.6	35, 36
Virginia Commonwealth U (MCV)	modified EGS4	Fast	21.8	34
U of Tübingen	XVMC	Fast		28
U of Leipzig	VMC	Fast		27
U of Michigan (RT_DPM)	modified DPM	Fast	7.3	33
U of California	PEREGRINE	Fast		26
Commercial				
BrainLAB, CMS and Elekta	XVMC	Fast	1.1	25
Nucletron and Varian	VMC++	Fast	0.9	25
NOMOS	PEREGRINE	Fast	43.3	25

Abbreviations: MCTP = Monte Carlo treatment planning system; Full = full Monte Carlo not using variance reduction technique (VRT) to keep the accuracy; Fast = fast Monte Carlo using VRT to reduce the calculation time.
* Calculation time with the in-house cluster system.

countries have developed in-house MC calculation systems, such as MCDOSE at Stanford University and Fox Chase Cancer Center, MCV at Virginia Commonwealth University, and MMCTP at McGill University (35-38). MCRTV was developed for clinical treatment plan verification, especially for routine quality assurance of IMRT plans. MCVS was originally developed for all of the high-precision radiotherapy treatment plans including the noncoplanar treatment plans for SBRT. All of the high-precision radiotherapy treatment plans should be verified with MC because of their complexity, but few institutions, especially in Japan, are able to do it.

We commissioned our clinical 6-MV photon beam phase-space data by determining, on the basis of the incident electron beam parameters, that MC calculations showed the best match with the measurements. Due to the inability to accurately correlate the ionization chamber reading with the dose in the build-up region and outside the region of flatness, accuracy of the estimation of the dose difference at these regions remains questionable (38). The differences were determined from the depth–dose curves for the region corresponding to each depth beyond the build-up region and from the lateral dose profile curves for each point of the off-axis within the region of flatness. Excellent agreements to within 1% between measurements and MC-calculated doses were obtained for the water phantom, except for the surface. There were wide variations among the incident electron beam parameters for MC models of 6-MV photon beams from the Varian linear accelerators (mean energy ranging from 5.7 MeV to 6.2 MeV and FWHM of radial intensity spread ranging from 0.10 cm to 0.20 cm, using a Gaussian beam model), even though many investigators determined on the basis of the incident electron beam parameters that MC showed the best match with the individual measurements. These variations can be partly attributed to several factors, such as individual differences among the accelerators and methods to model the treatment head components. Our results for the benchmarks under homogeneous conditions were consistent with these variations (41-44).

Relatively large differences between the dose distributions calculated with the MCVS and the commercial treatment planning systems were observed at the boundary of the tumor and the lung structures. This can be explained by inaccuracy of the conventional dose calculation algorithm due to heterogeneities. Dose perturbations at the interface between soft tissue and high- or low-density medium are due to a number of complex effects, which lead to the errors in dose computation associated with the conventional dose algorithms (5).

With the MCVS, high-precision radiotherapy treatment plans, such as 3DCRT, SBRT, and IMRT can be simulated. However, several aspects of the MCVS need to be explored, such as the tongue-and-groove effect and leaf leakage radiation through the Varian Millennium 120-leaf MLC. Actual measurements and those obtained with simulation need to be compared for validation of the MCVS.

CONCLUSIONS

Development of the MCVS was successful for performing MC simulations, including those for high-precision radiotherapy, 3DCRT, SBRT, and IMRT, as well as for analysis of calculated dose distributions. In this paper, we have presented the key features of the MCVS. The phase-space data of a 6-MV photon beam was developed, and several benchmarks were established under homogeneous conditions. The MC results showed good agreements with the actual measurements with discrepancies of 1% or less. However, measurements and simulations of the MLC-specific effects need to be compared for validation of the MCVS.

REFERENCES

1. Aspradakis MM, Morrison RH, Richmond ND, *et al.* Experimental verification of convolution/superposition photon dose calculations for radiotherapy treatment planning. *Phys Med Biol* 2003;48:2873–2893.
2. Starkschall G, Steadham RE, Popple RA, *et al.* Beam-commissioning methodology for a three dimensional convolution/superposition photon dose algorithm. *J Appl Clin Med Phys* 2000;1:8–27.
3. Liu HH, Mackie TR, McCullough EC. Calculating dose and output factors for wedged photon radiotherapy fields using a convolution/superposition method. *Med Phys* 1997;24:1714–1728.
4. DeMarco JJ, Solberg TD, Smathers JB. A CT-based Monte Carlo simulation tool for dosimetry planning and analysis. *Med Phys* 1998;25:1–11.
5. Ma CM, Mok E, Kapur A, *et al.* Clinical implementation of a Monte Carlo treatment planning system. *Med Phys* 1999;26: 2133–2143.
6. Carrasco P, Jornet N, Duch MA, *et al.* Comparison of dose calculation algorithms in phantoms with lung equivalent heterogeneities under conditions of lateral electronic disequilibrium. *Med Phys* 2004;31:2899–2911.
7. LoSasso T, Chui CS, Ling CC. Physical and dosimetric aspects of a multileaf collimation system used in the dynamic mode for implementing intensity modulated radiotherapy. *Med Phys* 1998;25:1919–1927.
8. van Santvoort JPC, Heijmen BJM. Dynamic multileaf collimation without "tongue-and-groove" underdosage effects. *Phys Med Biol* 1996;41:2091–2105.
9. Webb S, Bortfeld T, Stein J, *et al.* The effect of stair-step leaf transmission on the "tongue-and-groove problem" in dynamic radiotherapy with a multileaf collimator. *Phys Med Biol* 1997; 42:595–602.
10. Kim JO, Siebers JV, Keall PJ, *et al.* A Monte Carlo study of radiation transport through multileaf collimators. *Med Phys* 2001; 28:2497–2506.
11. Plessis FCP, Willemse CA, Lötter MG, *et al.* Comparison of the Batho, ETAR and Monte Carlo dose calculation methods in CT based patient models. *Med Phys* 2001;28:582–589.
12. AAPM TG-65. Tissue inhomogeneity corrections for megavoltage photon beams. AAPM Report No. 85. Madison (WI): Medical Physics Publishing; 2004.
13. International Commission on Radiation Units and Measurements. Determination of absorbed dose in a patient by beams of X or gamma rays in 485 radiotherapy procedures. ICRU Report 24. Bethesda (MD): 1976.
14. International Commission on Radiation Units and Measurements. Use of computers in external beam radiotherapy procedures with high-energy photons and electrons. ICRU Report 42. Bethesda (MD): 1987.
15. Ma CM, Pawlicki T, Jiang SB, *et al.* Monte Carlo verification of IMRT dose distributions from a commercial treatment planning optimization system. *Phys Med Biol* 2000;45:2483–2495.
16. Kong FM, Haken RKT, Schipper MJ, *et al.* High-dose radiation improved local tumor control and overall survival in patients with inoperable/unresectable non-small-cell lung cancer: Long-term results of a radiation dose escalation study. *Int J Radiat Oncol Biol Phys* 2005;63:324–333.
17. Rogers DWO, Walters BR, Kawrakow I, et al. BEAMnrc users manual. National Research Council of Canada Report PIRS-0509 (A) revK; 2007.
18. Rogers DWO, Walters BR, Kawrakow I, et al. DOSXYZnrc users manual. National Research Council Report PIRS-794 revB; 2007.
19. Fippel M, Haryanto F, Dohm O, *et al.* A virtual photon energy fluence model for Monte Carlo dose calculation. *Med Phys* 2003;30:301–311.
20. Walters BRB, Kawrakow I, Rogers DWO. History by history statistical estimators in the BEAM code system. *Med Phys* 2002;29:2745–2752.
21. International Commission on Radiation Units and Measurements. Tissue substitutes in radiation dosimetry and measurement. ICRU Report 44. Bethesda (MD): 1989.
22. Deasy JO, Blanco AI, Clark VH. CERR: A computational environment for radiotherapy research. *Med Phys* 2003;30:979–985.
23. Spezi E, Lewis DG, Smith CW. A DICOM-RT-based toolbox for the evaluation and verification of radiotherapy plans. *Phys Med Biol* 2002;47:4223–4232.
24. Siebers JV, Keall PJ, Libby B, *et al.* Comparison of EGS4 and MCNP4b Monte Carlo codes for generation of photon phase space distributions for a Varian 2100C. *Phys Med Biol* 1999; 44:3009–3026.
25. Reynaert N, van der Marck SC, Schaart DR, *et al.* Monte Carlo treatment planning for photon and electron beams. *Radiat Phys Chem* 2007;76:643–686.
26. Hartmann SCL, Walling RS, Daly TP, *et al.* Description and dosimetric verification of the PEREGRINE Monte Carlo dose calculation system for photon beams incident on a water phantom. *Med Phys* 2001;28:1322–1337.
27. Kawrakow I, Fippel M, Friedrich K. 3D electron dose calculation using a voxel Monte Carlo algorithm (VMC). *Med Phys* 1996;23:445–457.
28. Kawrakow I, Fippel M. Investigation of variance reduction techniques for Monte Carlo photon dose calculation using XVMC. *Phys Med Biol* 2000;45:2163–2184.
29. Fippel M, Kawrakow I, Friedrich K. Electron beam dose calculations with the VMC algorithm and the verification data set of the NCI working group. *Phys Med Biol* 1997;42:501–520.
30. Fippel M. Fast Monte Carlo dose calculation for photon beams based on the VMC electron algorithm. *Med Phys* 1999;26: 1466–1475.
31. Kawrakow I. VMC++, electron and photon Monte Carlo calculations optimized for radiation treatment planning. Advanced Monte Carlo for radiation physics, particle transport simulation and applications. In: A Kling, *et al.*, editors. Proceedings of the Monte Carlo 2000 Meeting. Lisbon, Portugal. Berlin: Springer; 2001. p. 229–236.
32. Cygler JE, Daskalov GM, Chan GH, *et al.* Evaluation of the first commercial Monte Carlo dose calculation engine for electron beam treatment planning. *Med Phys* 2004;31:142–153.
33. Sempau J, Wilderman SJ, Bielajew AF. DPM, a fast, accurate Monte Carlo code optimized for photon and electron radiotherapy treatment planning dose calculations. *Phys Med Biol* 2000; 45:2263–2291.
34. Siebers JV, Keall PJ, Kim JO, et al. Performance benchmarks of the MCV Monte Carlo system. In: Schlegel W, Bortfeld T, editors. Proceedings of the 13th International Conference on the Use of Computers in Radiation Therapy (ICCR) Heidelberg, Germany. Berlin: Springer; 2000. p. 129–131.
35. Ma CM, Li JS, Pawlicki T, *et al.* A Monte Carlo dose calculation tool for radiotherapy treatment planning. *Phys Med Biol* 2002;47:1671–1689.
36. Ma CM, *et al.* MCSIM: A Monte Carlo dose calculation tool for radiation therapy. In: Yi BY, Ahn SD, Choi EK, *et al.*, editors. Proceedings of the 14th International Conference on the Use of Computers in Radiation Therapy (ICCR). Seoul, Korea. Seoul: Jeong; 2004. p. 123–126.
37. Alexander A, DeBlois F, Stroian G, *et al.* MMCTP: a radiotherapy research environment for Monte Carlo and patient-specific treatment planning. *Phys Med Biol* 2007;52:N297–N308.
38. Yamamoto T, Mizowaki T, Miyabe Y, *et al.* An integrated Monte Carlo dosimetric verification system for radiotherapy treatment planning. *Phys Med Biol* 2007;52:1991–2008.

39. Wang L, Chui CS, Lovelock M. A patient-specific Monte Carlo dose-calculation method for photon beams. *Med Phys* 1998;25: 867–878.
40. American Association of Physicists in Medicine TG-105. Issues associated with clinical implementation of Monte Carlo-based photon and electron external beam treatment planning. AAPM Report No. 97. *Med Phys* 2007;32:4827.
41. Ding GX. Energy spectra, angular spread, fluence profiles and dose distributions of 6 and 18 MV photon beam: Results of Monte Carlo simulations for a Varian 2100EX accelerator. *Phys Med Biol* 2002;47:1025–1046.
42. Sheikh-Bagheri D, Rogers DWO. Sensitivity of megavoltage photon beam Monte Carlo simulations to electron beam and other parameters. *Med Phys* 2002;29:379–390.
43. Keall PJ, Siebers JV, Libby B, *et al.* Determining the incident electron fluence for Monte Carlo-based photon treatment planning using a standard measured data set. *Med Phys* 2003;30: 574–582.
44. Cho SH, Vassiliev ON, Lee S, *et al.* Reference photon dosimetry data and reference phase space data for the 6 MV photon beam from Varian Clinac 2100 series linear accelerators. *Med Phys* 2005;32:137–148.

Medical Design and Design Awards

Takashi Ogawa*, Toshikatsu Hunayama, Ichiro Kanaya, Kazuo Kawasaki
Osaka University
**takashi@design.frc.osaka-u.ac.jp*

1.Introduction

There is historical evidence in healthcare that the development of medical equipment/medical device found new test methods and treatment methods. And the design of medical equipment is considered to become important for future society as coping strategies against global aging and arrival of global infection. Therefore, the quality of medical equipment should be improved by evaluating the design of medical equipment from the viewpoint of therapeutic efficacy and security. For this purpose, design awards currently in place in each country is considered to be helpful.

However, there are few studies compiled about design award of medical equipment so far. Transition of design award winning equipment and trend of design award is not unambiguous.

Thus, in this writing, we will verify the history of design award and make clear the transition of equipment. In addition, we will make clear the trend of design award based on this transition. Furthermore, we will describe the perspective of future healthcare and design considering the utility of the role of design played in healthcare.

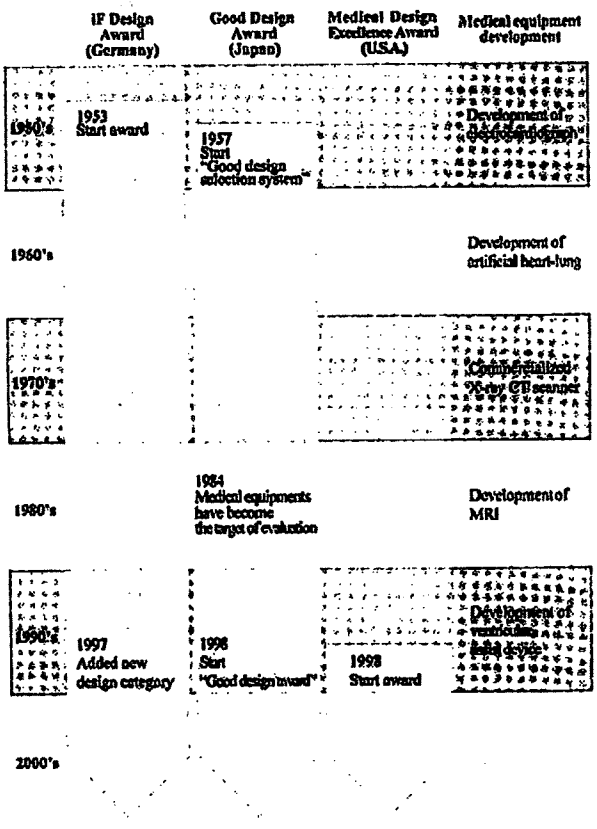

FIGURE: Chronology of design awards and medical equipment development

2. Study methods

2.1 Surveyed Design awards

Three awards of Good Design Awards (G mark prize), Insutrie Forum Design Hannover (iF design award), and Medical design Excellent Award (MDEA) will be subjected to study. There are four reasons for taking up these awards.

- The design award has history.
- The design award evaluates design of medical equipment.
- The design award is in place in each region of the world, such as Asia, Europe, and North America.
- The design award is aimed at products in each country.
- We will investigate the award-winning results of these design awards especially in 1954 and 1955, 1984, 1988, and 2007. There are three reasons for taking up these four periods.
- The period clarifies the design of medical equipment in early design age.
- Evaluation of the design of medical equipment was started in these periods.x

- The period helps foreseeing future development based on the recent award-winning trend.

Chronology of design awards and medical equipment development are shown in the table. (FIGURE)

2.2 Outline of Good design award

Good design award (G mark) system is a design award in Japan [1]. There are more than 1,000 award-winning products annually. G marks were awarded to 1,047 products entered in 2007. Good Design Award was started from "Good design selection system" established by the Ministry of International Trade and Industry in 1957. Since 1984, the award system has broadened the scope of its activity with all industrial products as target of evaluation. Medical equipments have become the target of evaluation at this phase. The system was privatized in 1998, and the award is named as "Good Design Award" hosted by Japan Industrial Design Promotion Organization up to the present date. The evaluation is roughly categorized as follows [2].

- Product design
- Architecture and Environment Design
- Communication Design
- New Frontier Design
- Asean Design

Medical equipment is handled in Product Design category. Criterion for evaluation is divided into three main stages. [3]

- Is it a good design? (The basic elements required of a Good Design product or facility)
- Is it a superior design? (Considerations that make the superior aspects of the product or facility)
- Is it a design that breaks new groud for the future?(Considerations for evaluating whether the design actively engages issues having to do with the future life, industry, and society.)

There are few design awards in the world with such detailed criterion.

2.3 Outline of iF design award

iF design award is a German design award hosted by Industrial Forum Design Hannover, which is annually awarded to more than 800 products; in 2007, iF award was presented to 821 entered products [4]. IF design award was established in 1953 as "Die gute Industrieform" [5]. The name was changed in 1990 to the current name of "iF Industrial Forum Design Hannover". The hosting system was changed in 1997; various categories have been targeted for design award in addition to the existing iF product design award. Medical equipment has been targeted for evaluation since the beginning of the award. Criterions for evaluation are eleven categories.

- Design quality
- Workmanship
- Choice of material
- Degree of innovativeness
- Environmental compatibility
- Functionality
- Ergonomics
- Visualization of use
- Safety
- Brand value / branding
- Universal design

2.4 Outline of Medical design excellence award

Medical design excellence award (MDEA) is an American design award targeted for design of medical equipment hosted by a private company, Canon Corporations LLC, with publishing as a main business[6]. About 30 products are awarded annually. The first evaluation was in place in 1998, and is still in place today. Design award specialized in the design of medical equipment is unique on a global basis. Criterions for evaluation are six categories.

- Innovative use of materials, components, or processes in the fabrication of the product.
- The ability of the product development team to overcome design and engineering challenges so that that product meets its clinical objectives.
- User-related design and engineering features that improve health care delivery, with special attention to functional innovations that broaden the scope of users, change

traditional medical attitudes or practices, or offer significant use-related improvements.

- Design and engineering features that provide enhanced benefits to the patient (e.g., comfort, fit, service access, safety, appropriate aesthetics, overall improvement of health care).
- Aspects of product design and engineering that improve the manufacturer's profitability.
- Product features that improve the overall delivery of healthcare

3. Result

3.1 Beginning design awards - 1953, 1954

Dominant design award was IF product award only in this period in early design period. Total number of awarded products of iF product design award was 221. Number of awarded medical equipment among them was only one. Products targeted for award was a medical operating table.

Total number of awarded products was increased to 394 in the following year; four medical equipments were awarded. Products targeted for award were orthodontic appliance, thermometer, hearing aid, and dental drill case; products from medical equipment to welfare apparatus in current classification were targeted in this phase.

3.2 Period of design award – 1984

Medical equipment was targeted for evaluation as G mark this year. Total number of awarded products of iF award was 360. Number of awarded medical equipment among them was seven. Products targeted for award was centered on electronic medical equipment such as X-ray diagnostic apparatus, magnetic resonance imaging device, dental implement, respiratory monitoring equipment, and transmitter/receiver of pacemaker. But, all of them awarded were provided by Siemens AG.

On the other hand, total number of awarded products of G mark was 1341, among which 34 products were awarded in medical category. Awarded products were comprised of imaging system such as X-ray diagnostic apparatus, and specialized equipment such as laser surgical equipment. Commercialized products such as dumbbell and consumer sphygmomanometer were also awarded at the same time. Among them, four overseas manufacturer's products were also awarded.

3.3 Spread of Medical design - 1998

Total number of awarded products of iF design award was 394. Number of awarded medical equipment among them was 27. Awarded products were comprised of X-ray diagnostic apparatus and laser surgical equipment always awarded in the past. In addition, we can focus on the point that artificial heart lung apparatus, directly linked to life, is also awarded. Equipment based on QOL of patient such as rehabilitation apparatus and wheelchair is also targeted for the award.

And the number of products awarded for G mark was 855. Medical equipment was categorized as "Clinic, Health and welfare" category this year. Number of products awarded in this category was 37. Product awarded a good design gold prize, evaluated as excellent design, was automated teller machine; a product different from so-called medical equipment was highly evaluated. Some imaging systems were awarded, however, mixture of products categorized in welfare apparatus such as hearing aid and Braille plate, and hospital facility such as nurse call were awarded.

The total number of awarded products of MEDA started this year was 18. Awarded products were comprised of apparatus related to physical invasiveness such as syringe pump and infusion device. This award is unique in presenting award to portable stretcher related to emergency medical care, which is different from other awards.

3.4 During recent year - 2007

Total number of awarded products of iF award increased greatly to 754. Medical equipment, welfare apparatus, etc. were integrated this year into Medical + health care category, and 20 products were awarded. Awarded products were comprised of various products such as imaging system, joint supporter, in vitro clinical test equipment, medical information monitor. Products manufactured by Japanese manufacturers were also awarded. Equipments directly related to medical treatment awarded include only incubator; relatively more products categorized as welfare apparatus were awarded.

In G mark, medical equipment and welfare apparatus were categorized in different categories this year. Total number of awarded products was 1043, among which 20 products were awarded in facilities, and systems for medical institutions category. Awarded products were comprised of the existing imaging system, however, products based on the needs of healthcare professionals

such as tape holder were awarded. A product in very limited category such as bone clamp used for operation by a doctor was entered and awarded. It is unique that design of medical system is also among the target of award in a new frontier design category, which is different from facilities, and systems for medical institutions.

Total number of awarded products in MEDA was 18. The awarded products were comprised of brain surgical apparatus as well as facility in a hospital such as in vitro clinical test equipment. It is marked by evaluating advanced medical care and equipment for its purpose.

4. Discussion

4.1 Comparison of awarded products in each design award by period

Throughout all the period, advanced and valuable imaging system is awarded. As performance of such system is improved in a cycle of several years, the design is renewed in each case, which enables consecutive award winning in similar equipments.

German iF award is profound in evaluating design of advanced products such as electronic equipment irrespective of the early period of design award in 1954.

In 1984, medical equipment category in iF award is stagnant, and it is peculiar that only one company was awarded. Meanwhile, from this year in Japan, not only general consumer products but also medical equipment and hospital facility were targeted for evaluation, which shows the expansion of design field related to health such as from imaging system to dumbbell in several manufacturers.

In 1998, wheelchair was awarded in iF award. It is assumed that not only providing product simply equipped with required function but also designing of the product has become improved. In Japan, there is no award winning of products directly related to human life such as medical treatment equipment. Meanwhile, in foreign countries, relation of maturity in design and healthcare in each country can be seen in the fact that artificial heart lung and surgical instrument were awarded.

From 2007, not only products used in hospital but also equipments used in each scene of daily living are designed. The fact shows the beginning of reflection of needs that keeps good health in everything in one's life.

4.2 Future perspective of design for medical equipment

Number of awarded design of equipment related to medical treatment is few from the beginning. With harsh evaluation required, improvement of evaluation method for advanced approach as well as tightening selection method in design award is considered necessary. As a result, treatment process and its related equipment/system may become awarded with design award for medical care itself.

5. Conclusion - Recent development of medical equipment category in each country

Evaluation for new treatment method and device can be seen in America. Products based on the needs of healthcare professionals are coming in Japan. New design area is being established in medical equipment and in a scene of daily life in Germany.

However, there are few awards winning for surgical instruments, etc. Introduction of design for equipment related to treatment is required. Although system design for medical care is different from one nation to another, evaluation of medical equipment, etc. should be performed through international design award. In addition, the design, which promotes medical care in developing countries, should be implemented, and the system should promote it by holding design award.

NOTES

(1) Japan Industrial Design Promotion Organization, G mark *taizen* - Good design *shyu no Gojyunen*, Japan Industrial Design Promotion Organization, 2007.

(2) Good Design Award, (http://www.g-mark.org/) June .1 2008.

(3) Shiro Aoki, Discovery of New Evaluation Measure in Judgement of Good Design Award , SPECIAL ISSUE OF JSSD, Vol.6, No. 4, Japan Society for the Science of Design , Tokyo, 1996.

(4) iF – International Forum Design Hannover: Homepage (http://www.ifdesign.de/) June .1 2008.

(5) Editorial Committee, World Design Awards-iF Design Awards (Germany), SPECIAL ISSUE OF JSSD, Vol.6, No. 4, Japan Society for the Science of Design , Tokyo, 1996.

(6) Home|MedicalDesignExcellenceAwards (http://www.devicelink.com/expo/awards06/home/) June .1 2008.

A basic discussion to introduce design methodology to the development of the artificial heart

Toshikatsu Funayama, Takashi Ogawa, Ichiro Kanaya, Kazuo Kawasaki
Osaka University
funayama@design.frc.eng.osaka-u.ac.jp

The design methodology

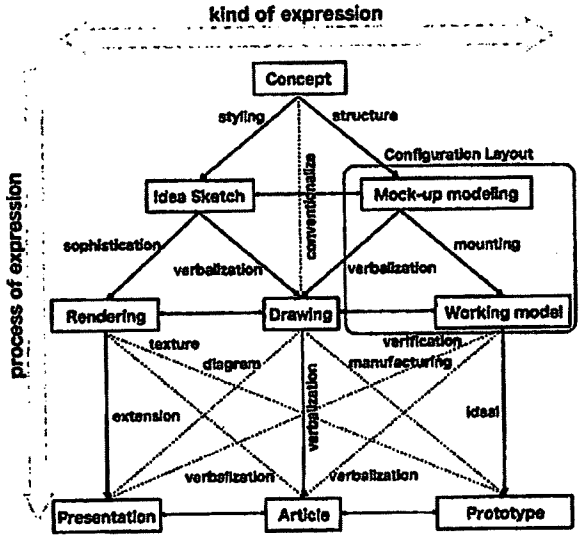

kind of expression

process of expression

	KOTOBA 1 dimension	2 dimension	KATACHI 3 dimension
idea	Concept	Idea Sketch	Mock-up modeling
expression	Drawing	Rendering	Working model
communication	Article	Presentation	Prototype

Kazuo Kawasaki model 1st-3rd

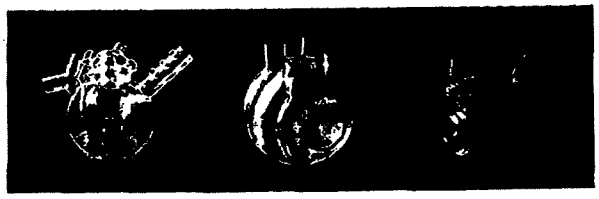

FIGURE: Design Methodology and Kazuo Kawasaki model 1st-3rd

Background

Treatment for patients with severe end-stage cardiac failure due to a heart disease includes "heart transplantation" based on the Brain Death and Organ Donation Law and "artificial heart implantation". However, social issues concerning lack of hearts to be donated and ethical situation of the society remain in the former. Thus, development of artificial hearts has been anticipated.

At present, artificial hearts are roughly divided into two; "assistant artificial heart" and "total artificial heart". The former is fitted for the purpose of assisting the pump function in the left or right heart or both while preserving the natural heart of the patient. The latter, in contrast, is implanted in the place of the natural heart that has been taken out. Development of artificial hearts has a long history in comparison to other artificial organs but no definite conclusion or solution has been reached yet. They have been developed mainly by cooperation of medicine and engineering and introduction of design has been neglected completely. Design methodology is "an approach to manufacture a product together with the techniques and knowledge to be materialized" and the design methodology alone cannot achieve final production. Engineering technology is essential for industrialization. In other words, it is an approach that enables academic cooperation with other fields.

This study is intended to supplement what lacks in the present cooperation of medicine and engineering and to propose a new development system by smoother cooperation focusing to design by introducing the design methodology to the development of artificial hearts, especially to advance materialization of "total artificial heart".

Method

Based on the research and development of artificial hearts so far and actual historical events, hypothesis will be formulated assuming that the "design methodology" was introduced already to the artificial hearts developed in the past. From the hypothesis, excesses and shortages found in the research and development as well as materialization will be extracted to discuss and examine how to introduce the design methodology.

The design methodology used here refers to all imaginary